



Assessing the upcycling potential of construction and demolition waste derived silt: Activation, physicochemical and mineralogical characterisation

Surya Maruthupandian¹ , Andreas Chrysanthou², Antonios Kanellopoulos^{3,*} 

Centre for Engineering Research, School of Physics, Engineering and Computer Science, University of Hertfordshire, Hatfield, UK

ARTICLE INFO

Keywords:

CDW derived silt
Construction and demolition waste
Upcycling
Mineral waste
Supplementary cementitious materials

ABSTRACT

The increase in infrastructure requirements of modern urban societies has led to repair, retrofitting or demolition of existing buildings producing enormous amounts of construction and demolition waste (CDW). Processing and recycling of fine fractions from CDW is an area of research with growing interest, primarily due to the mineralogy of such waste fines that make them potential candidates to be utilised within binder systems (cement-based or alkali-activated). The utilization of fine waste from CDW recycling in cementitious binders necessitates a deeper understanding of its physical, mineralogical, and chemical composition in order to enhance confidence in its application. Therefore, this study focuses on characterisation and developing a suitable treatment for CDW derived silt for its use as a binder precursor. To achieve this, the physical, chemical, mineralogical and pozzolanic properties of CDW derived silt were studied and mechanochemical activation (high energy milling) and thermal activation (calcination) were adopted to enhance its reactivity. The findings from XRD, FTIR, elemental composition, and examination of microstructure of treated and untreated samples collectively revealed alterations in the mineral phases and morphology resulting from the treatment processes. The reactivity of the activated samples was evaluated by examining their solubility in an alkaline environment using ICP-OES and measuring their heat of hydration using adapted R3 tests. It was determined that the samples calcined at 750°C exhibited a higher heat of hydration and a greater concentration of soluble silicon (Si) and aluminium (Al) in sodium hydroxide solution.

1. Introduction

Construction and demolition waste (CDW) refers to the waste generated during the construction, retrofit, and demolition of buildings and infrastructure. It is a significant source of waste generation worldwide, accounting for a substantial percentage of the total waste generated in many countries. Rapid urbanisation and upgrade of national infrastructures are responsible for the vast amounts of CDW. In the year 2016, the European Union (EU) alone generated about 374 million tonnes and according to the European Commission, CDW accounts for approximately one third of total waste generated within the EU [1]. At the same time the equivalent amount for the UK was 66.2 million tonnes [2,3]. Future projections are not encouraging either. According to a

report by the United Nations Environment Programme (UNEP), global CDW generation is expected to double by 2025, reaching an estimated 2.2 billion tonnes per year [2].

Past studies explored the possibility of reuse of CDW in construction as coarse aggregates and fine aggregates in the manufacture of concrete [3–5]. This approach faces a significant number of technological challenges; at the same time the processing of such wastes to produce aggregates is always associated with production of silt, powder waste and other forms of waste which cannot be used in construction directly [6,7]. Processing of fine fractions from CDW is an area of research and development with growing interest, primarily due to the mineralogy of such waste fines that makes them good potential candidates to be utilised within binder systems (cement-based or alkali-activated).

* Corresponding author.

E-mail address: a.kanellopoulos@herts.ac.uk (A. Kanellopoulos).

¹ <https://orcid.org/0000-0001-7408-2641>

² <https://orcid.org/0000-0001-9554-5676>

³ <https://orcid.org/0000-0001-9278-2035>

<https://doi.org/10.1016/j.conbuildmat.2025.143163>

Received 8 May 2025; Received in revised form 7 July 2025; Accepted 11 August 2025

Available online 16 August 2025

0950-0618/© 2025 The Author(s). Published by Elsevier Ltd. This is an open access article under the CC BY license (<http://creativecommons.org/licenses/by/4.0/>).

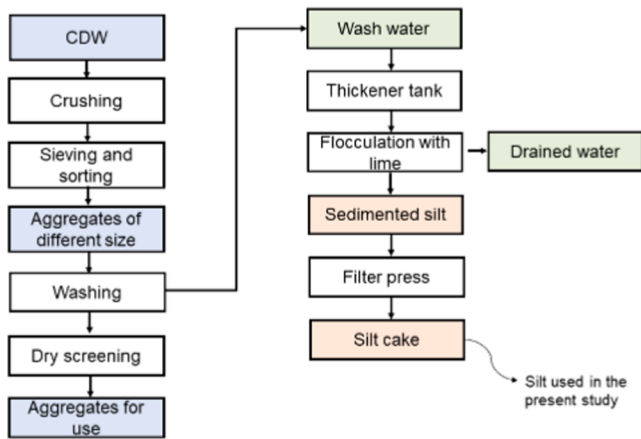


Fig. 1. Process of silt formation in the CDW recycling plant which was used for sampling in this study.

However, these fine fractions are typically of low reactivity, and this necessitates the implementation of processing techniques that will yield these by-products suitable for cementitious action [8]. There is some work in this domain, but it is still an emerging area of research and development that calls for widespread and more systematic studies [9–13]. Developing upcycling procedures for this waste stream will not only create environmental benefits by reducing landfilling of

CDW-derived silt but will also benefit the cement manufacturing industry by providing alternative and more environmentally friendly binder compounds.

Silt is defined as a loose granular substance resulting from natural erosion or from splitting of larger rock and sand particles [14]. The unified soil classification system grades silt between 0.002 and 0.063 mm and the Krumbein phi scale defines silt as particles within a size range 0.0039–0.0625 mm [14]. Some studies also considered industrial wastes and by-products of this particle size range as silt [15–17]. There are also investigations that assessed the possibility of geopolymerisation of silt waste originating from CDW recycling. Naturally-occurring silt contains minerals such as quartz, feldspars, chlorites micas and carbonates along with clay minerals and is similar to mineral wastes like mine tailing, fly-ash and GGBFS [18–20] [21,22]. It was observed that the composition of the silt makes it suitable for alkali activation when used alone or in combination with fly-ash or silica fume. Compressive strengths in the range of 15 MPa to 40 MPa were achieved by varying the NaOH molarity from 4 to 10 and a curing temperature of 60°C.

The present study focuses on characterisation of CDW generated silt to assess its potential for upcycling within cementitious binder systems. To achieve this, mechanical, chemical and thermal treatments were deployed for processing the silt.



Fig. 2. Colorimetric comparison of silt, cement, silica fume and fly ash.

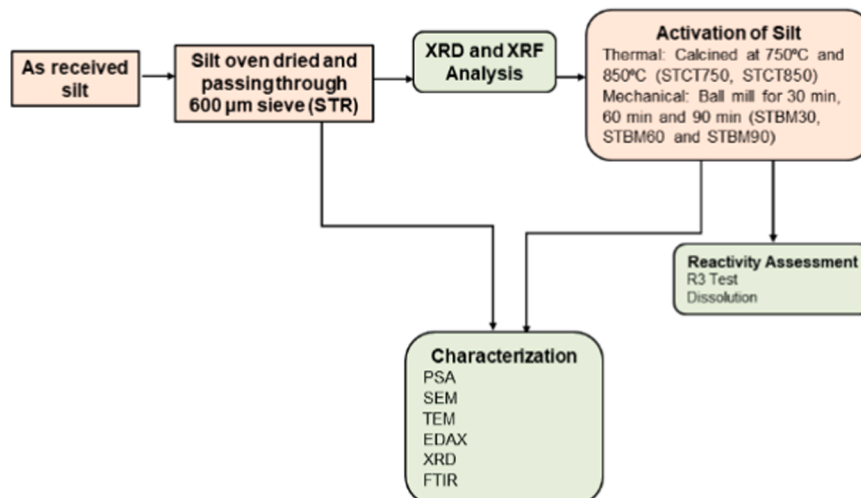


Fig. 3. Experimental methodology process followed in this study.

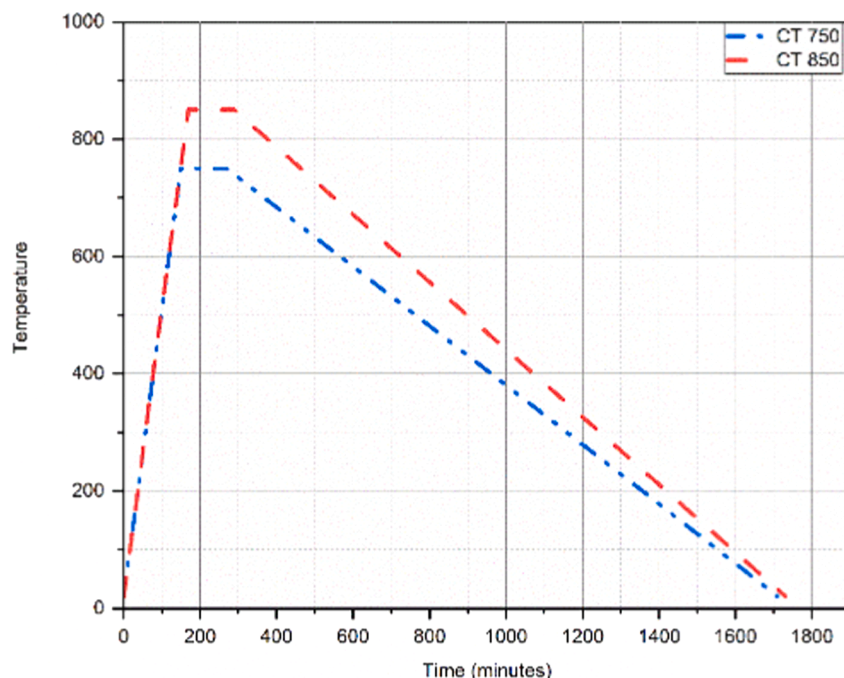


Fig. 4. Heat treatment adopted in the study (CT 750 and 850 indicates samples calcined at the temperatures 750 °C and 850 °C respectively).

2. Materials

2.1. Silt

The silt used in the study was collected from a construction waste recycling plant located in Hertfordshire, UK. The plant processes aggregates generated from construction and demolition waste which are washed, and this wash water is treated in a thickener tank with a flocculant (typically aluminium or iron salts). The silt settled in the thickener tank is mixed with lime solution. The reason for this is that the lime solution reacts with any clay present in silt and enhances solid sedimentation and facilitates better drainage in the filter. The mixture is filled in filter press and clear water is drained away. The filter is left with silt in the form of filter cakes. The process adopted [23] is summarised schematically in Fig. 1. The material obtained from the plant had a few lumps which, prior to any testing, were broken, and oven dried at 80°C for 24 h, sieved through 600 µm sieve and used for further tests. The drying regime (temperature and duration) was selected based on trials until the material attained constant weight.

Fig. 2 shows a visual comparison of silt (STR), cement, fly ash and silica fume. The silt in its raw form is a brown powder denoted as 5YR 6/4 as per Munsell scale whereas fly ash, cement and silica fume were denoted as N4, N5 and 4PB5/3 respectively [24].

2.2. Chemicals and reagents

In this study, laboratory-grade chemicals and reagents were used. For dissolution studies, sodium hydroxide solution of the required molarity was prepared using deionized water and sodium hydroxide pellets of 98 % extra pure grade from Acros Organics. For the pozzolanic activity (R3) tests, 85 % extra pure potassium hydroxide flakes, 98 % pure calcium hydroxide, and 99 % pure granular potassium sulphate from Acros organics were used, along with calcium carbonate precipitate in powder form procured from Fisher Scientific.

Concentrated hydrochloric acid (Fisher Scientific), of a specific gravity of 1.18 and a concentration 37 %, was used to prepare a 1 M solution to adjust the pH of the leachate for studies on dissolution. To create this 1 M solution, concentrated HCl was diluted with deionized

water. During analytical studies, isopropyl alcohol was used for dispersion and cleaning to prevent contamination (SEM, TEM, ICP, XRD). For benchmarking, commercially available fly ash and silica fume were used. For calibration purposes during dissolution studies, Si and Al ICP standard solutions (Reagecon Diagnostics) with concentration 1000 mg/mL in HNO₃ were used. Rietveld analysis performed to quantify the amount of the amorphous phase present in the silt using anatase from Thermo Scientific with a purity of 98 + % as an internal standard.

3. Experimental methodology

Following the identification of the mineral phases present in the silt, the activation methods and the associated parameters were chosen. Following activation, the treated silt was characterized and compared to the characteristics of raw silt (referred to as STR in this study) to better understand the changes in properties with treatment.

To prevent lumps and achieve sample uniformity, the raw silt was oven dried at 80°C for 24 h and sieved through a 600 µm sieve. The oven-dried sample was used for the additional tests covered in Sections 3.1 to 3.5 after being stored in airtight containers and placed in a vacuum chamber. The samples were further ground using a mortar and pestle to a size finer than 150 m to prepare it for tests that called for finer samples. Fig. 3 depicts a summary of the experimental design used in this study.

3.1. Particle size

A laser particle size and particle distribution instrument (HELOS/KF with RODOS dry dispersion) was used to measure the particle size distribution of the unprocessed and ball-milled samples. A lens (R5) that covers the size range between 0.5 and 875 µm, was used for this test.

3.2. Microstructural analysis and mineralogy

Morphology and microstructure of the samples were studied using JSM-5700F, JEOL scanning electron microscope (SEM) run at 20 kV. The powder samples were dispersed on carbon tape and sputter coated

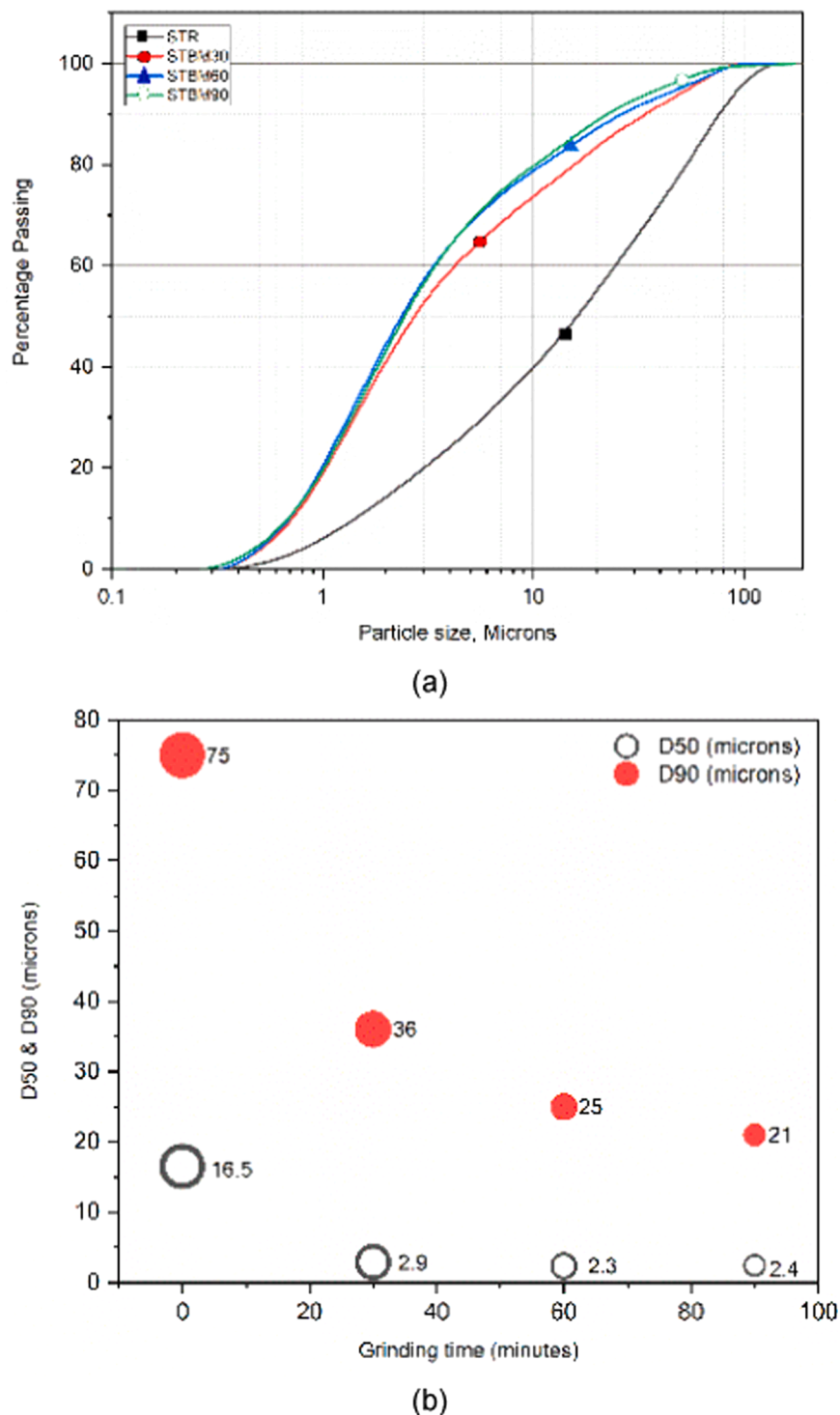


Fig. 5. Particle size analysis of milled and as received CDW derived silt (a) Particle size distribution of samples before and after milling and (b) Decrease in D₉₀ and D₅₀ values with increase in milling time.

with gold. To determine the elements present, EDAX energy-dispersive X-ray microanalysis was also carried out. Based on tests, an acceleration voltage of 15 kV and a spot size of 47 μm were chosen to produce a clear image. In this study, the average of two EDAX spot analyses is reported.

JEOL JEM-1400F transmission electron microscope (TEM) at 200 kV, was used to observe physical and morphological changes in the individual particles resulting from the applied treatment. Samples for TEM were prepared as follows: 1 g of silt sample was mixed with

isopropyl alcohol in a test-tube until it formed a colourless suspension. This suspension was subjected to 20 kHz ultrasonication for one minute. Using a micropipette, a drop of this dispersed sample was mounted on a holey carbon grid. The isopropyl alcohol was allowed to completely evaporate by drying the grid at 27°C for three hours in an environment chamber.

Panalytical Zetium WDXRF (Wavelength Dispersive X-ray Fluorescence) and Panalytical SuperQ software, was used to determine the oxide composition of the silt. The data was calibrated using the WROXI

Table 1

Oxide composition of graphite mine tailing used in the present study in comparison with oxide composition of as-received silt used in this study, benchmark silt from literature (for comparison purposes), fly ash, silica fume, GGBFS and cement.

Oxides	As-received silt	Silt – Benchmark [22,30]	Fly ash [31]	Silica Fume [31]	GGBS[31]	Cement [32]
SiO ₂	56.87	54.00–98.00	48.20–51.90	94–98	33.00–37.00	19.30
Al ₂ O ₃	10.16	7.90–12.40	26.00–30.10	0.1–0.4	8.00–35.00	3.70
Fe ₂ O ₃	5.53	4.60–5.80	5.50–11.30	0.02–0.15	0.50–2.00	4.10
Na ₂ O	0.45	0.80–1.30	1.0–3.70	0.1–0.4		0.28
MgO	1.25	0.30–0.70		0.3–0.9	6.00–14.00	2.10
K ₂ O	1.67	2.00–3.30		0.20–0.70		0.88
CaO	21.00	3.00–18.40	2.10–4.20	0.08–0.30	34.00–43.00	63.20
SO ₃	1.39	0.10–0.90	0–0.10		0.80–2.00	4.00
TiO ₂	0.71	0.60–0.80				0.29
BaO	0.48					
Mn ₃ O ₄	0.06	0.10			0.30–1.10	
V ₂ O ₅	0.02					
ZnO	0.02					
ZrO ₂	0.04					
Cr ₂ O ₃	0.00					
CuO	0.00					
NiO	0.02					
P ₂ O ₅	0.29					0.17
PbO	0.00					

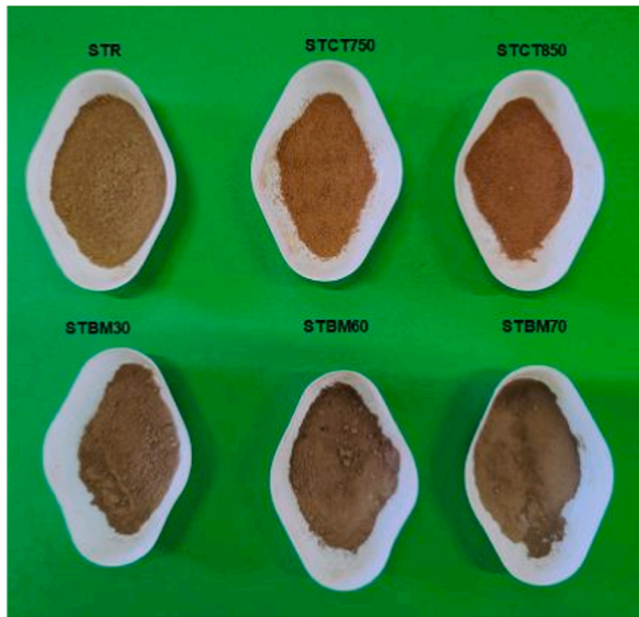


Fig. 6. Appearance of silt before and after activation. Note: CT refers to calcined CDW derived silt and BM refers to ball milled CDW derived silt.

(wide-ranging oxides) standard to calculate the oxide concentration in weight percentage.

To study the mineralogy, X-ray diffractometry was carried out using a Bruker D8 Advance X-ray diffractometer (XRD) with Cu-K radiation at a wavelength of 1.540549 Å and an energy of 8.04 keV. Silt samples were sieved through a 150 µm sieve prior to XRD analysis to remove large particles causing any preferential orientation and to produce a smooth surface. A glass plate was used to strike off the excess fine powder and create a flat, smooth surface after it had been spread out on the XRD sample holder. The XRD results were analysed using HighScore Plus X-ray diffraction software [25].

To determine the phase composition and functional groups, FTIR studies were carried out. A Shimadzu IRSPIRIT infrared spectrometer equipped with LabSolutions IR Spectrum software was used. In this study, 16 scans between 4000 cm⁻¹ and 600 cm⁻¹ were performed on each sample. Silt passing the 150 µm sieve was used for the FTIR

samples.

To assess the efficiency of the calcined temperature and correlate with the rest of the experimental observations the as-received CDW derived silt samples passing the 600 µm sieve were investigated thermogravimetrically. For this purpose, a TGA 8000 thermogravimetric analyser by Perkin Elmer was used in nitrogen environment between 50 °C and 1100 °C at a heating rate of 10 °C per minute. The evolved gases were continuously analyzed using Spectrum Two FTIR Spectrometer (LiTaO₃ Detector). For each sample, 4 scans were performed between 4000 cm⁻¹ and 600 cm⁻¹ using the LabSolutions IR Spectrum software.

3.3. Activation of silt

3.3.1. Mechanical activation

The materials were milled to reduce their size and activate them mechanically. A Fritsch Pulversette 6 planetary ball mill was used for the milling. The XRD analysis of the raw silt revealed the presence of minerals with a Mohs hardness range of 2–7. To prevent wear and tear of the balls and jar and subsequent contamination of the material, grinding media with hardness higher than the material was chosen. A tungsten carbide grinding jar and balls with a hardness of 9 on the Mohs scale were used.

According to the literature [26], after 20 min of milling, the integral intensity of crystalline peaks would decrease and after 80 min, the crystallinity of quartz, albite (plagioclase), and muscovite would also decrease [26]. Based on this information, milling times of 30 min (MTBM30), 60 min (MTBM60), and 90 min (MTBM90) were adopted in the present study. The amount of kinetic energy imparted during milling is directly proportional to the diameter of the balls raised to the power of four. As the maximum particle size of the material used for grinding is anticipated to be less than 600 µm after sieving, the largest suitable size of 10 mm balls was used to optimize the diameter and impart maximum collision energy (kinetic energy) [27]. A ball to powder ratio of 2.5 was adopted.

3.4. Thermal activation

Based on the mineralogy and observations from past literature, the calcination temperatures were chosen. The calcination temperatures were selected to be 750°C and above because the initial XRD showed the presence of calcite and illite. It has been previously reported that, heating above 900°C results in the formation of new crystalline alumin-

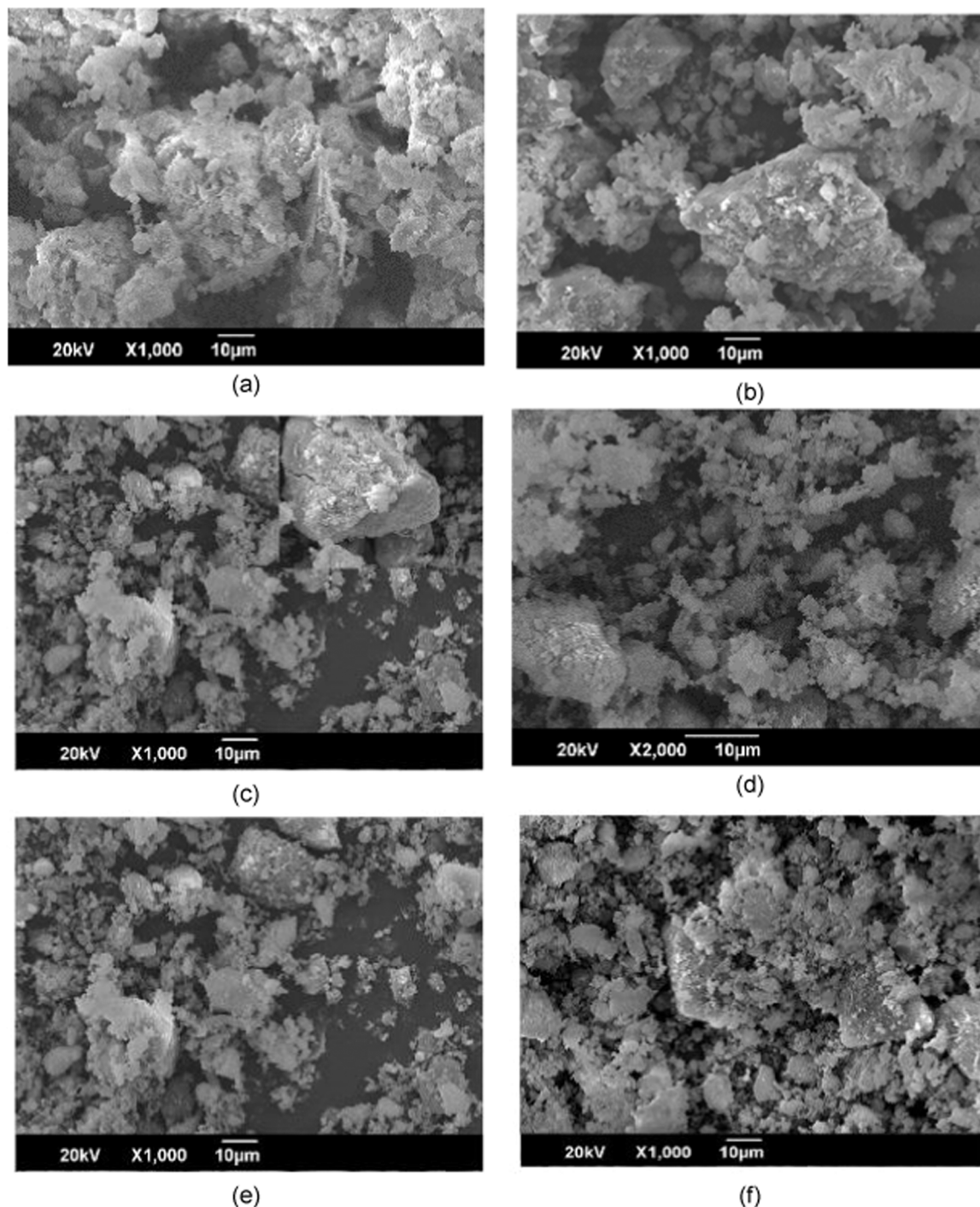


Fig. 7. SEM images of samples used in this study. (a) STR; (b) STCT750; (c) STCT850 (c) Inner image – appearance of crack during calcination in STCT850; (d) STBM30; (e) STBM60; (f) STBM90 (f) Inner image - A few large sized particles observed after milling contributing to selective grinding in STBM90. Note: CT refers to calcined CDW derived silt and BM refers to ball milled CDW derived silt.

silicate mineral phases, which may negatively affect the reactivity of activated silt [28]. Hence, calcination temperatures of 750°C, and 850°C were adopted to decompose the crystalline phases. The samples calcined at these temperatures are referred to as STCT750, and STCT850, respectively.

Calcination was performed using a tray-shaped fused alumina crucible with internal measurements of 217 mm × 95 mm × 60 mm and a wall thickness of 16 mm. The material was evenly distributed in the crucible to a height of 15 mm to ensure even heating of the sample. To accommodate the thermal expansion of the crucible and avoid fracture

from thermal shock, a ramp up rate of 300°C/hour was used. To ensure complete calcination, the samples were kept at the predetermined temperature for two hours. To prevent thermal shock (to the samples, the crucibles and the heating elements) caused by rapid cooling, the samples were left to cool down to room temperature in the furnace. Fig. 4 depicts the entire calcination cycle.

3.5. Dissolution of Si and Al

Si and Al availability for condensation and gel formation in an alkali-

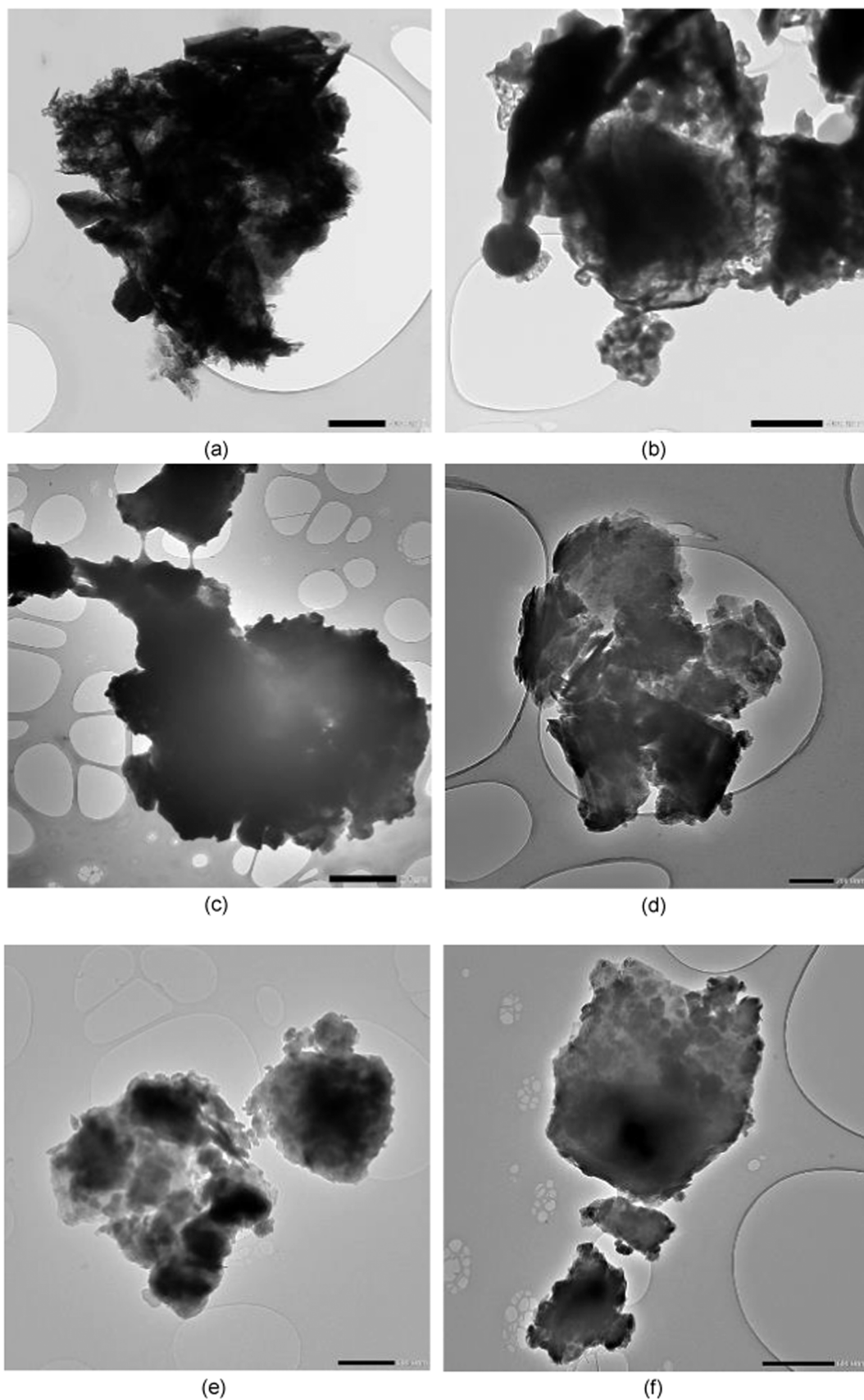
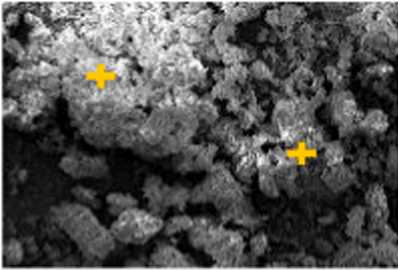
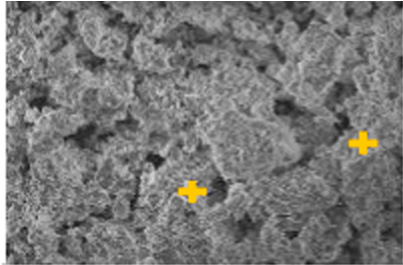
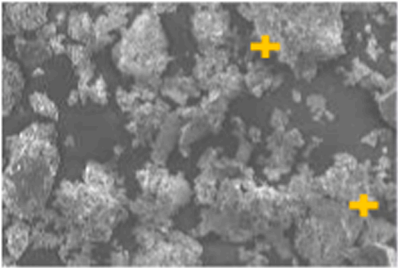
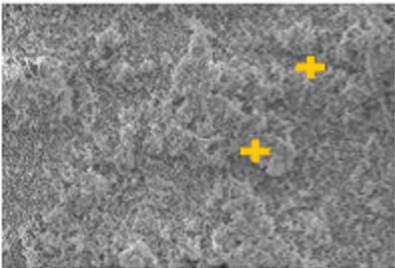
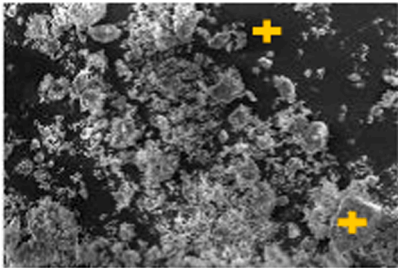
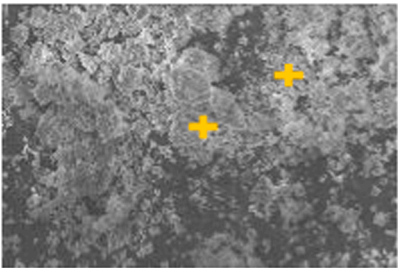
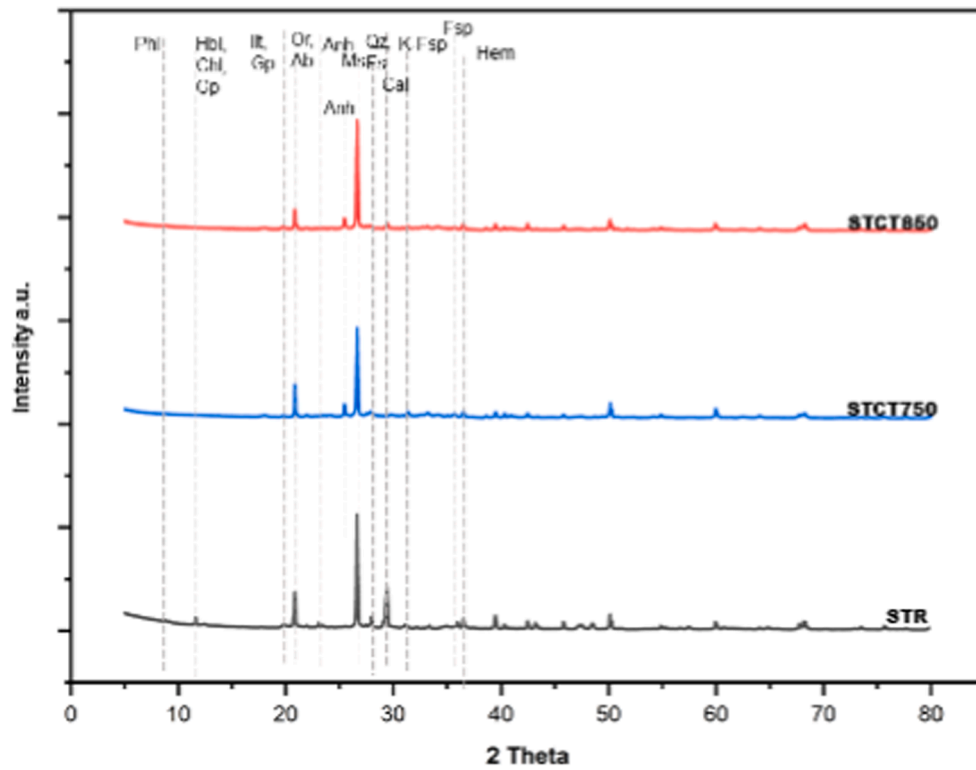


Fig. 8. TEM images of untreated and processed silt samples. (a) STR; (b) STCT750; (c) STCT850; (d) STBM30; (e) STBM60; (f) STBM90. Note: CT refers to calcined CDW derived silt and BM refers to ball milled CDW derived silt.

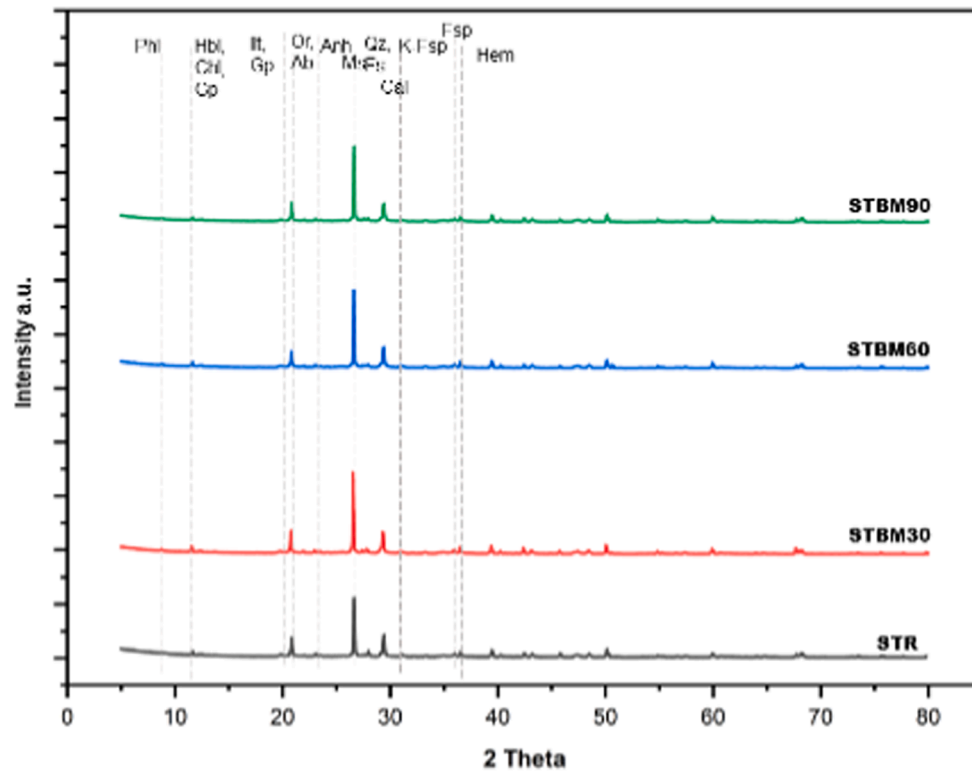
Table 2

Elemental composition of the raw and the treated silt samples.

Sample ID	Image	Elemental Composition		
STR		Element	Weight (%)	Atom (%)
		O	52.96	69.21
		Na	0.57	0.52
		Mg	1.19	1.02
		Al	6.90	5.35
		Si	19.76	14.71
		S	1.43	0.94
		K	1.25	0.67
		Ca	11.34	5.91
		Fe	3.78	1.42
STCT750		Element	Weight (%)	Atom (%)
		O	35.38	53.10
		Na	0.44	0.46
		Mg	0.97	0.965
		Al	7.60	6.76
		Si	22.54	19.27
		S	2.32	1.74
		K	2.27	1.40
		Ca	24.11	14.44
		Fe	4.375	1.885
STCT850		Element	Weight (%)	Atom (%)
		O	48.02	66.61
		Na	0.70	0.67
		Mg	1.64	1.50
		Al	7.54	6.20
		Si	16.19	12.79
		S	2.01	1.39
		K	0.75	0.42
		Ca	7.74	4.28
		Fe	15.42	6.13
STBM30		Element	Weight (%)	Atom (%)
		O	37.78	56.24
		Na	0.52	0.54
		Mg	1.14	1.12
		Al	8.29	7.32
		Si	20.57	17.45
		S	2.51	1.87
		K	2.04	1.25
		Ca	15.86	9.43
		Fe	11.31	4.83
STBM60		Element	Weight (%)	Atom (%)
		O	45.29	63.55
		Na	0.75	0.73
		Mg	1.36	1.26
		Al	6.85	5.70
		Si	17.64	14.11
		S	3.14	2.20
		K	1.95	1.11
		Ca	13.22	7.41
		Fe	9.82	3.95
STBM90		Element	Weight (%)	Atom (%)
		O	44.36	62.18
		Na	0.79	0.77
		Mg	1.24	1.14
		Al	7.35	6.11
		Si	19.72	15.75
		S	2.50	1.75
		K	1.66	0.95
		Ca	14.93	8.36
		Fe	7.46	3.00



(a)



(b)

Fig. 9. XRD phases of silt samples before and after activation. (a) calcined samples (b) ball milled samples. Phl – Phlogopite, Hbl – Hornblende, Cl – Chlorite, Gp – Gypsum, Ill – Illite, Or – Orthoclase, Ab – Albite, An – Anhydrite, Ms – Muscovite, Qz – Quartz, Fs – Ferrosilite Fsp- Feldspar, Cal – Calcite, K-Fsp - K-feldspar, Hem – Haematite. Note: CT refers to calcined CDW derived silt and BM refers to ball milled CDW derived silt.

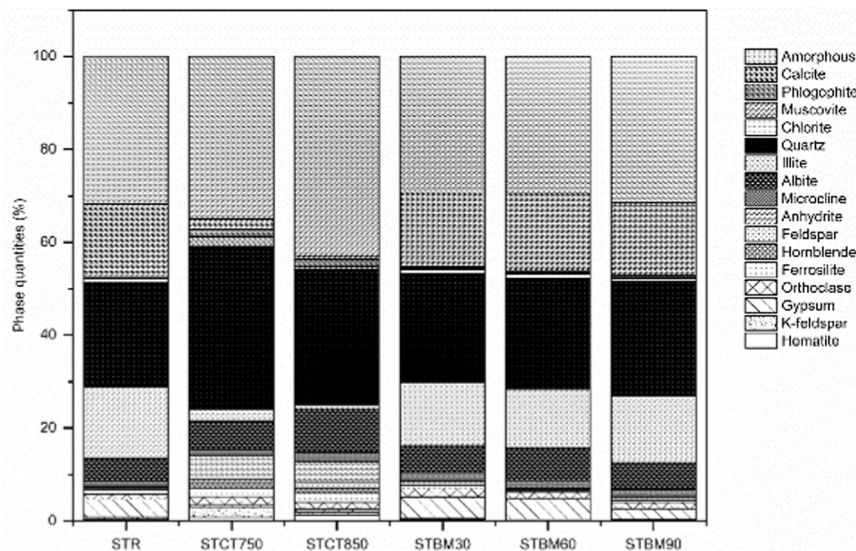


Fig. 10. Mineral phases and their respective quantities. Note: CT refers to calcined CDW derived silt and BM refers to ball milled CDW derived silt.

activated system is well indicated by their solubility in NaOH. It is possible to determine the suitability of activated tailing for alkali-activated binders by determining the solubility of Si and Al.

The solubility tests were conducted with 8 M NaOH. 50 g of alkaline solution was added to 1 g of material and mixed with a magnetic stirrer for 6 h. A 45 μm pore size filter paper was used to filter the solution after stirring. Deionized water was used to dilute this filtrate at a ratio of 1:50. To stop the ions from settling, this diluted leachate was acidified to a pH of 2 using 1 M HCl. The quantity of Si and Al leached into the alkaline solution from the mineral waste were determined using an Inductive Coupled Plasma Optical Emission Spectrometer (ICP-OES) equipped with a sea spray nebulizer and SPS3 autosampler.

3.6. Pozzolanic activity (adapted R3)

A rapid, relevant and reliable (R3) test was used to evaluate the pozzolanicity (chemical reactivity) of the treated silt. The test is performed in a simulated cementitious matrix environment following the general guidelines outlined in ASTM C1897 (2020). A solution of potassium hydroxide and potassium sulphate was prepared and added to a mixture of mineral waste, calcium hydroxide, calcium carbonate.

As recommended, the heat of hydration from the first 75 min after mixing were not taken into consideration to allow the calorimeter temperature to stabilize [32–34]. To minimize the difference in temperature all the materials and the containers used were conditioned at 60 °C for 24 h prior to the start of the procedure. Cumulative heat, at the end of seven days, per gram of material was reported. The higher heat of hydration indicates a higher degree of reactivity.

An I-Cal HPC - High Performance Calorimeter, was used to record the heat of hydration of this mixture over the course of seven days at a constant temperature. However, the test was performed at a modified temperature of 60 °C instead of 40 °C. Due to the low reactivity observed in STR samples, the heat of hydration results for these samples in the R3 test were rather low when the test was performed at 40 °C; this resulted in heat flow values indistinguishable from system noise. It has been reported [29] that the latent hydraulic reaction and pozzolanic reactions in the presence of calcium hydroxide can be activated by increase in temperature. Therefore, the test temperature was increased from 40 °C to 60 °C consequently enhancing the reactivity of non-reactive and less reactive materials [29]. Nevertheless, it is important to note that performing the test at an elevated temperature results in a reduction in the recorded heat of hydration [29] and this makes it difficult to compare the results to R3 test values obtained from

literature. To address this, in addition to the mineral waste samples, for benchmarking purposes the R3 test was performed at 60 °C for silica fume and fly ash which are known for their reactivity in cementitious systems.

4. Results and discussion

4.1. Particle size distribution

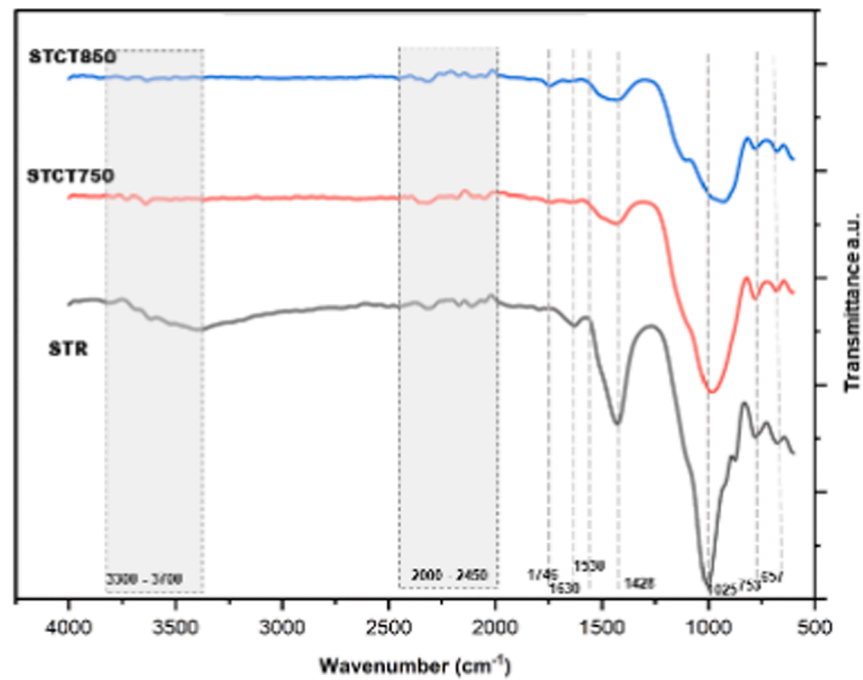
The findings of the particle size analysis of STR and the CDW derived silt after milling are reported in Fig. 5(a) and (b). The figures show that the silt used in the study was a fine material with 90 % of particles being finer than 75 μm . It can be observed from Fig. 5(a) that the STR was uniformly graded, and the particle size decreased with milling. However, the effect of milling on the reduction of particle size was less prominent after 30 min of milling. As presented in Fig. 5(b), the D_{50} and D_{90} values decreased by 52 % and 82 % respectively after 30 min, while a decrease of 66.7 % and 86 % were recorded after 60 min, and 72 % and 85.5 % after 90 min of milling. It is also apparent that the particle size of finer size particles slightly increased with milling after 60 min indicating agglomeration of particles.

4.2. Chemical composition, microstructure, and mineralogy

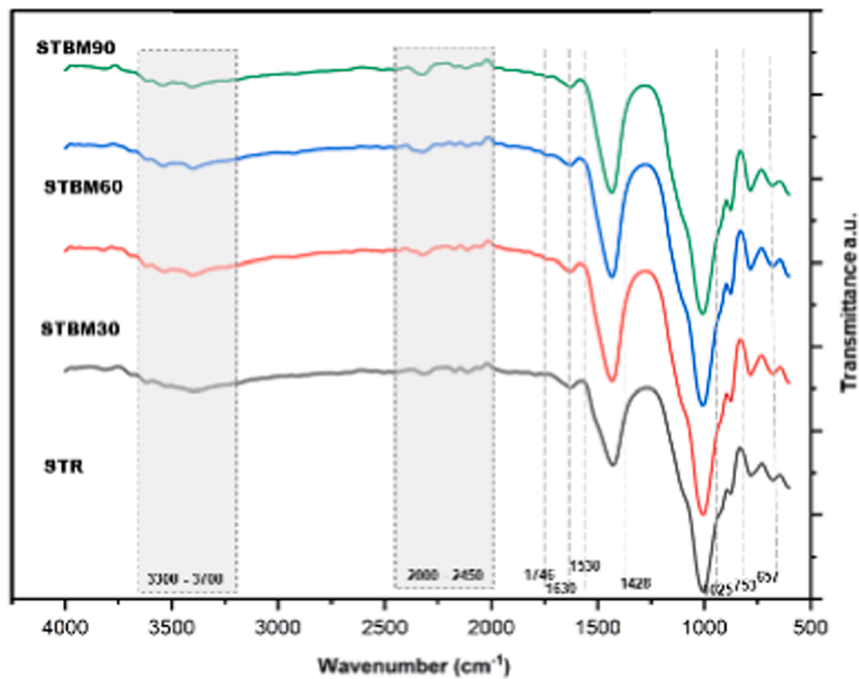
The chemical composition of the as received silt is shown in Table 1. Silica and calcium oxides are the major oxides present in the as-received material. Silts typically do not contain such large amounts of CaO but the use of lime in the treatment process adopted in the CDW plant resulted in a high percentage of CaO in the waste silt. The silica content was found close to that of fly ash and the calcium oxide content was about 10 % less than GGBS. It also contains about 10.2 % alumina and 5.5 % ferric oxide. The other minor contents present include oxides of potassium, magnesium, and sulphur in the range of 1.25 – 1.67.

A visual observation indicated that STR samples were brown coloured and calcined samples turned to brick red colour. This can be attributed to the oxidation of Fe present in the material. An image of treated and raw silt presented in Fig. 6.

The SEM images of the silt microstructure are presented in Fig. 7(a) to (f). The as received CDW derived silt (STR) was crystalline with particles of varying size. The large sized particles were rounded, whereas smaller particles were flaky or needle-like. It can be inferred that the rounded particles could be quartz, the needle-like particles are composed of calcium carbonate in aragonite form [33] and the flaky



(a)



(b)

Fig. 11. FTIR spectra of silt before and after activation. (a) calcined samples, (b) ball-milled samples. Note: CT refers to calcined CDW derived silt and BM refers to ball milled CDW derived silt.

particles are irregular shapes of phyllosilicates [34]. This observation is in line with the results of other studies where a similar mineralogy was reported [21,22,33,34].

The calcination of silt affected the physical morphology of the particles. The changes are apparent in Fig. 7(a) to (c). As the temperature of

calcination increased from 750°C to 850°C the needle-like structures disappeared due to decomposition of calcium carbonate during calcination, supporting the assumption that the observed mineral is calcium carbonate. There is also evidence of the formation of cracks in the material because of calcination. The appearance of cracks or flocculant

Table 3

FTIR absorbance bands and assignments.

Wavelength (cm ⁻¹)	Assignment	Reference
667–795	Si-O-Si symmetrical stretching	[42,39, 42]
950–1200	Asymmetric stretching of Al-O and Si-O	[43,44, 45]
1600 – 1700	Bending vibration H-O-H	[41,45]
1620, 1680	Gypsum	
3500, 2100–2200	Triple covalent C bonds	[46]
599.28, 1091, 1643, 3060 and 3091	C-OH, C-H, CO, C-C, OH bonds corresponding to oxidation reduction of graphite	
2200–3600	Stretching and bending of O-H	[44,45, 47]

appearance of particles after calcination are consistent with the findings of Zhao et al. [35] in their calcined materials [35]. Micrographs of the ball-milled ST samples are presented in Fig. 7(d) to (f). The average particle size decreased when compared to the STR samples with the exception for some large-sized particles. This can be attributed to the selective grinding due to difference in the grindability index of different minerals and the large particles could be composed of quartz which is of higher hardness [36].

Individual crystals were observed using TEM as shown in Fig. 8(a) to (f). The primary particle observation indicated that the silt particles were polycrystalline. Silt particles appeared to have softer edges and irregular shape. It can also be observed that the particles appear to have been composed of smaller particles with internal voids. Samples STCT750 and STCT850 exhibit formation of necking as shown in Fig. 8 (c). This could be due to primary crystallites forming solid bridges during the calcination process [37]. The milled samples STBM30, STBM60 and STBM90 appeared with rounded edges.

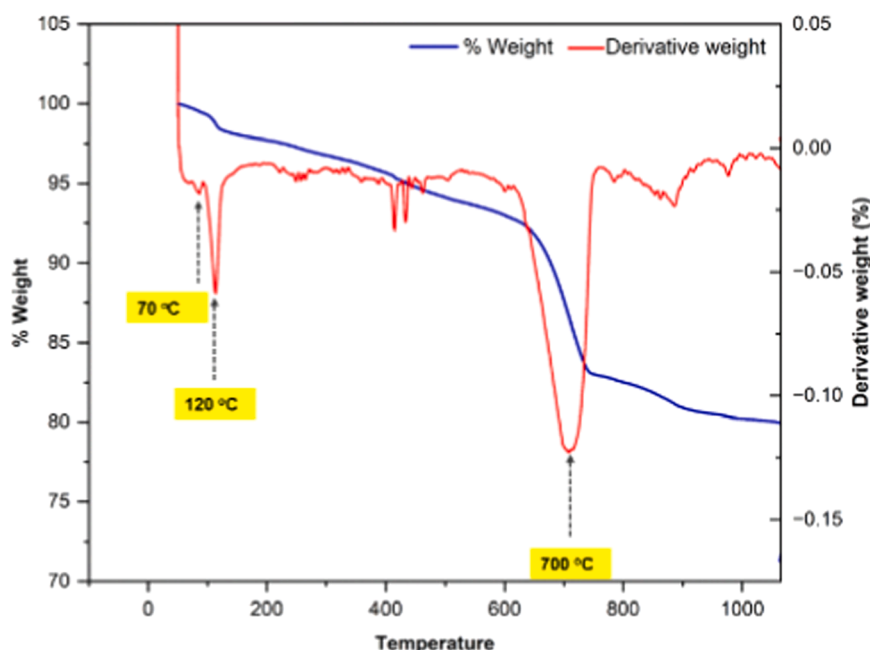
The results of EDAX analysis are presented in Table 2 and show that Si, Ca, Al and Fe were the major elements present. There was no significant change in the elemental composition because of the adopted treatment process.

The X-ray diffractograms (Fig. 9) indicated that the silt samples were highly crystalline. The phases and their corresponding COD reference ID [25] identified from XRD analysis are as follows: Haematite

(96–101–1268), K-Feldspar (96–155–7002), Gypsum (96–500–0040), Orthoclase (96–900–0163), Ferrosilite (96–900–0356), Hornblende (96–900–1227), Feldspar (96–900–3089), Anhydrite (96–900–4097), Microcline (96–900–4192), Albite (96–900–9664), Illite (96–900–9666), Quartz (96–900–9667), Chlorite (96–901–0166), Muscovite (96–901–2887), Phlogopite (96–901–3832), Calcium carbonate (96–901–6707). The peaks corresponding to calcium carbonate disappear upon calcination and this is also confirmed by the Rietveld quantification given in Fig. 10, where the calcium carbonate percentage decreased from 15.5 % in STR to 2.2 % in STCT750 and 0.86 % in STCT850. Similarly, dehydroxylation of illite occurs upon calcination and there is reduction in the amount of illite from 15.3 % to 2.59 % at 750 °C and from 15.3 % to 0.97 % at 850 °C. The increase in the amount of haematite was associated with the dehydroxylation of illite. The iron in illite usually exists as both Fe²⁺ and Fe³⁺; the Fe²⁺ (or FeO) form oxidized to haematite as reported in previous studies [20,38]. The dehydroxylation of illite also led to formation of amorphous silica and alumina and then the traces of iron present in the illite oxidises to form haematite. The milling of samples did not lead to any significant changes to the phase quantities or to formation of new phases.

The FTIR spectra for silt samples before and after activation are shown in Fig. 11 (a) and (b). The peaks have been assigned based on the literature and is given in Table 3.

According to the data presented in Table 3, the peaks observed at 657 cm⁻¹ and 773 cm⁻¹ are indicative of symmetrical stretching of Si-O-Si bonds. This can be designated to quartz, and these peaks remain without undergoing any substantial changes following activation. The peaks associated with the asymmetric stretching of Al-O and Si-O, located at 950 cm⁻¹, become combined with the prominent peak at 1025 cm⁻¹, and are only discernible in calcined samples after the decrease in intensity of the 1025 cm⁻¹ peak. This observation as depicted in Fig. 11 (a) reveals an asymmetrical peak at 950 cm⁻¹ in calcined samples, accompanied by the formation of a shoulder in the spectral region corresponding to a wavenumber of 1250 cm⁻¹. The observed peak at 1025 cm⁻¹ can be attributed to the in-plane stretching of Si-O bonds in illite [39]. In calcined samples, this peak is observed to broaden, which can be attributed to the dehydroxylation process of illite where the crystal structure shifts from an ordered to disordered orientation. This observation is supported by the observed reduction in the quantity of illite as determined through XRD analysis. The peak

**Fig. 12.** TGA Analysis of STR.

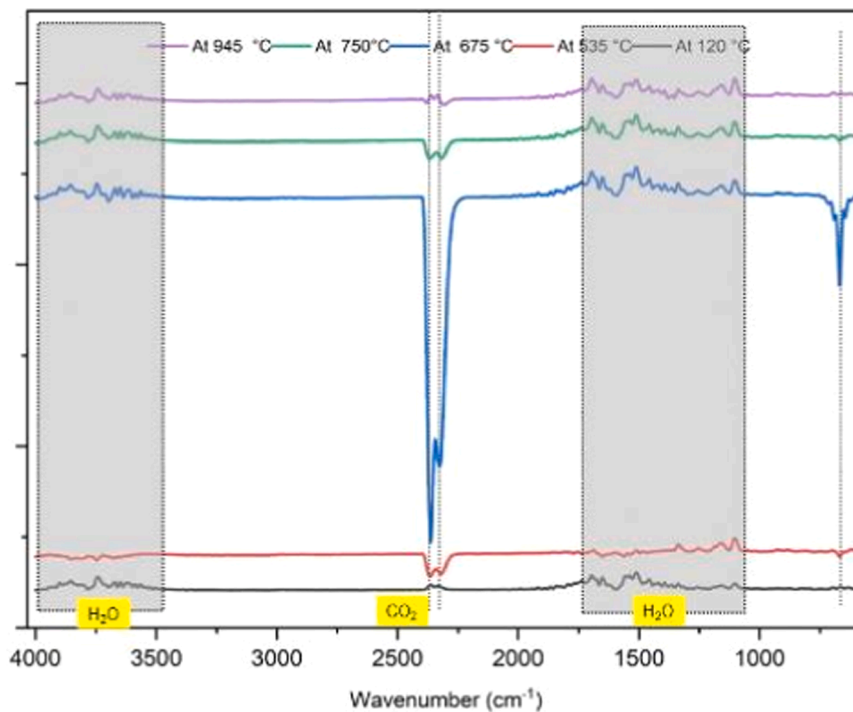


Fig. 13. FTIR spectra of evolved gases during TG analysis.

observed at 1428 cm^{-1} can be attributed to the presence of C-O bonds in calcite [40]. This peak is not observed in calcined samples indicating the decomposition of calcite and is consistent with the results obtained from XRD analysis. The peaks at wavenumbers 1558 cm^{-1} and 1653 cm^{-1} are indicative of the bending vibrations of the H-O-H bond. The peaks observed in the range of $2000\text{--}2450\text{ cm}^{-1}$ and $3300\text{--}3700\text{ cm}^{-1}$ correspond to the bending and stretching vibrations of the H-O-H molecule [39]. However, the spectra exhibit a flattened appearance in this region for calcined samples, suggesting the occurrence of dehydration in gypsum and dehydroxylation in illite and a range of OH species from other phases removed during calcination. The peaks at 1620 cm^{-1} , 1680 cm^{-1} , 3526 cm^{-1} and 3402 cm^{-1} corresponding to gypsum [41] disappear with calcination as observed in Fig. 11 (a). This observation is further supported by the results of XRD analysis where the illite and gypsum peaks disappear upon calcination and Rietveld analysis indicates changes in quantities of these phases.

In Fig. 11 (b) the FTIR spectra for ball milled samples demonstrated a decrease in relative peak intensities of approximately 38 % after the milling process. The peaks at 657 cm^{-1} and 773 cm^{-1} indicate Si-O-Si bonds of quartz and remain without any significant alterations after milling. The peaks associated with the asymmetric stretching of Al-O and Si-O, located at 950 cm^{-1} combined with the prominent peak at 1025 cm^{-1} which corresponds to the in-plane Si-O bonds of illite [39]. The peak at 1428 cm^{-1} corresponding to C-O bonds in did not show any significant changes upon milling. The peaks at wavenumbers 1558 cm^{-1} and 1653 cm^{-1} are indicative of the bending vibrations of the H-O-H bond. The peaks observed in the range of $2000\text{--}2450\text{ cm}^{-1}$ and $3300\text{--}3700\text{ cm}^{-1}$ correspond to the bending and stretching vibrations of the H-O-H molecule and peaks at 3526 cm^{-1} and 3402 cm^{-1} correspond to gypsum [39]. These peaks remain unchanged even after the milling process.

The relative weights and the differential weights of the STR sample between $50\text{ }^{\circ}\text{C}$ and $1100\text{ }^{\circ}\text{C}$ are given in Fig. 12. The weight loss between $100\text{ }^{\circ}\text{C}$ and $140\text{ }^{\circ}\text{C}$ corresponds to partial dehydration of gypsum to form hemi-hydrate, while the loss between $140\text{ }^{\circ}\text{C}$ and $200\text{ }^{\circ}\text{C}$ corresponds to dehydration of hemi-hydrate to form anhydrite. The steep weight loss between $625\text{ }^{\circ}\text{C}$ to $700\text{ }^{\circ}\text{C}$ is attributed to the decomposition

of dolomite ($\text{CaMg}(\text{CO}_3)_2$) [48,49]. Leading to $700\text{ }^{\circ}\text{C}$, dolomite decomposes to MgO and mildly crystalline calcium oxide which then reacts further, similar to CaCO_3 decomposition, leading to the formation of more calcium oxide and CO_2 . This second part occurs at lower temperature than the decomposition temperature of pure calcite (around $800\text{ }^{\circ}\text{C}$) due to the poor crystallinity of CaO. Weight loss continues beyond $700\text{ }^{\circ}\text{C}$, where the calcite starts decomposing. These observations are in line with the chemical analysis (Table 1) and XRD results where the reduction in percentage of calcite was observed with calcination. The thermal decomposition of illite occurs at around $800\text{ }^{\circ}\text{C}$.

The analysis of the evolved gases in Fig. 13 shows emission of water and CO_2 during calcination. The evolved gas analysis at a temperature of $675\text{ }^{\circ}\text{C}$ shows a stronger CO_2 peak at $2000\text{--}2500\text{ cm}^{-1}$ confirming the decomposition of calcite. The water is loss associated with the dehydration of gypsum and clay minerals.

4.3. Pozzolanic activity

The heat of hydration of the silt samples is given in Fig. 14. The findings of R3 tests in previous studies [29,50] suggest that the initial high heat of hydration that is followed by slower or almost no heat of hydration is a typical trend of a highly reactive supplementary cementitious material. It can be observed from Fig. 14 that the behaviour of silica fume fits this description. In addition, a gradually increasing heat of hydration is typical of a slow reactive pozzolan such as fly ash.

Results in Fig. 14 (a) and (b) show that STR, STBM60 and STBM90 are almost inert. Though STCT750 and STBM60 were having a heat of hydration lower than fly ash and silica fume, they performed comparatively better than the other samples. This signals that in these two cases a degree of pozzolanicity is expected. The heat of hydration of fly ash was about 2.4 times that of STCT750 and 2.6 times that of STBM60. Similarly, the heat of hydration of silica fume was about 1.8 times that of STCT750 and 2 times that of STBM60. These observations are in line with heat of hydration measurements reported in the literature on similar CDW derived fine materials intended for cementitious action [10,12].

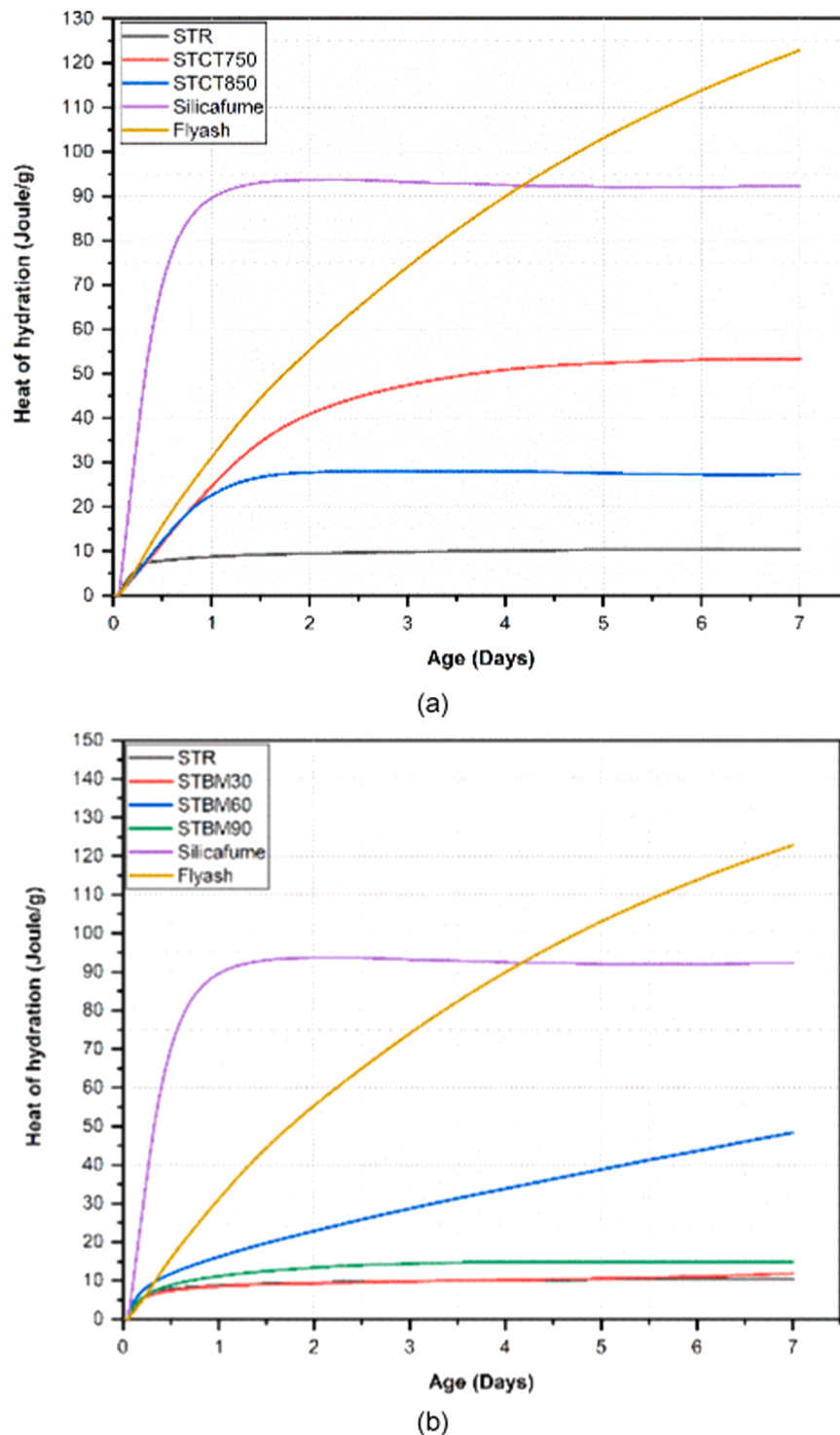


Fig. 14. Heat of hydration from pozzolanicity test of silt at 60 °C. (a) calcined samples (b) ball milled samples. Note: CT refers to calcined CDW derived silt and BM refers to ball milled CDW derived silt.

4.4. Dissolution of Si and Al

The solubility of Si and Al in 8 M NaOH is obtained from ICP-OES. This gives an indication of Si and Al available for formation of hydration products in an alkaline environment and hence the value is directly proportional to the reactivity of the material in an alkali activated cement or in a binder system [30]. The results of the test are reported in Fig. 15 and show that STCT750 had a higher solubility, 9 mg/L of Si and 1.05 mg/L Al than the other samples (3.3 – 4.5 mg/L of Si and

0.36–0.45 mg/L). This signals that the silt samples calcined at 750°C (STCT750) shall have more Si and Al available in the matrix for reaction in case of alkali activation.

5. Conclusions

The present study evaluated the possibility of upcycling CDW derived silt that exists in the form of filter cakes. These filter cakes were generated while filtering the wash water during the processing of CDW

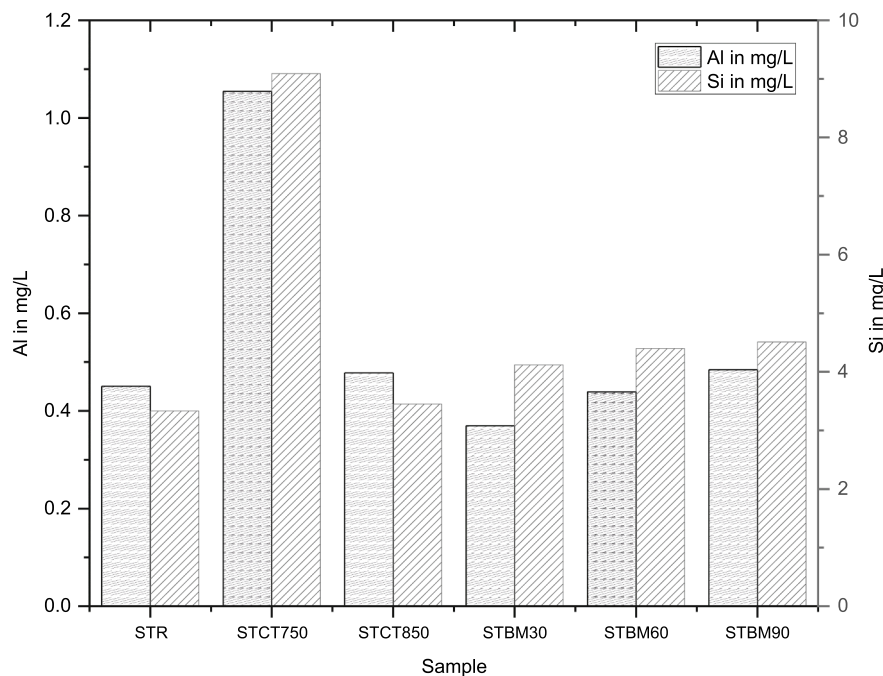


Fig. 15. Solubility of Si and Al from raw, calcined and ball milled CDW derived silt in 8 M NaOH. Note: CT refers to calcined CDW derived silt and BM refers to ball milled CDW derived silt.

in a dedicated plant facility. This paper presented characterization studies of raw and activated silt. The findings of the study showed that the silt was mainly composed of silica and calcium oxide. The mineral composition of the raw silt was studied, and the phases present suggested a possibility of activation by calcination and high energy milling. The activation process altered the morphology and performance of the material. The silt calcined at 750 °C performed better than the other samples.

The results of the pozzolanicity tests showed that silt calcined at 750 °C had higher heat of hydration suggesting that it can be used as a supplementary cementitious material. In addition, it exhibited better dissolution of Si and Al making it more suitable for use in alkali activated cements as a source of Si and Al.

The findings of the study are encouraging for use of silt in a cementitious binder. It also indicated that mineralogical composition is the most important factor in the determination of the activation methods and the feasibility of further use of the material. Thus, from the study, it can be recommended that a case specific mineralogical study should be performed to assess the feasibility of further use and selection of suitable activation methods.

Statements and declarations

This project has received funding from the European Union's Horizon 2020 research and innovation programme under the Marie-Sklodowska-Curie grant agreement No - 801604. The authors would like also to express their gratitude to Dr Theodore Hanein and Dr Aniruddha Baral of the University of Sheffield, for their help with the XRF data.

CRediT authorship contribution statement

Surya Maruthupandian: Writing – original draft, Investigation, Formal analysis, Data curation. **Antonios Kanellopoulos:** Writing – review & editing, Supervision, Project administration, Funding acquisition, Data curation, Conceptualization. **Andreas Chrysanthou:** Writing – review & editing, Supervision.

Declaration of Competing Interest

The authors declare that they have no known competing financial interests or personal relationships that could have appeared to influence the work reported in this paper.

Data availability

Data will be made available on request.

References

- [1] Construction and demolition waste, (n.d.). https://environment.ec.europa.eu/topics/waste-and-recycling/construction-and-demolition-waste_en (accessed April 2, 2023).
- [2] U.N.E. Programme, Disaster Waste Management Mechanism: A Practical Guide for Construction and Demolition Wastes in Indonesia, (2008). <https://wedocs.unep.org/xmlui/handle/20.500.11822/27292> (accessed April 2, 2023).
- [3] B. Wang, L. Yan, Q. Fu, B. Kasal, A comprehensive review on recycled aggregate and recycled aggregate concrete, *Resour. Conserv. Recycl.* 171 (2021) 105565, <https://doi.org/10.1016/j.resconrec.2021.105565>.
- [4] G. Bai, C. Zhu, C. Liu, B. Liu, An evaluation of the recycled aggregate characteristics and the recycled aggregate concrete mechanical properties, *Constr. Build. Mater.* 240 (2020) 117978, <https://doi.org/10.1016/j.conbuildmat.2019.117978>.
- [5] M. Surya, V.V.L.K. Rao, P. Lakshmy, Mechanical, durability, and time-dependent properties of recycled aggregate concrete with Fly ash, *Acids Mater. J.* 112 (2015) 653–661, <https://doi.org/10.14359/51687853>.
- [6] L. Qiao, Y. Tang, Y. Li, M. Liu, X. Yuan, Q. Wang, Q. Ma, Life cycle assessment of three typical recycled products from construction and demolition waste, *J. Clean. Prod.* 376 (2022) 134139, <https://doi.org/10.1016/j.jclepro.2022.134139>.
- [7] M. Behera, S.K. Bhattacharyya, A.K. Minocha, R. Deoliya, S. Maiti, Recycled aggregate from C&D waste & its use in concrete - a breakthrough towards sustainability in construction sector: a review, *Constr. Build. Mater.* 68 (2014) 501–516, <https://doi.org/10.1016/j.conbuildmat.2014.07.003>.
- [8] M. Frías, R. Vigil De La Villa, S. Martínez-Ramírez, L. Fernández-Carrasco, E. Villar-Cocina, R. García-Giménez, minerals Multi-Technique Characterization of a Fine Fraction of CDW and Assessment of Reactivity in a CDW/Lime System, (n.d.). <https://doi.org/10.3390/min10070590>.
- [9] D.O. de Lima, D.S. de Lira, M.F. Rojas, H.S. Junior, Assessment of the potential use of construction and demolition waste (CDW) fines as eco-pozzolan in binary and ternary cements, *Constr. Build. Mater.* 411 (2024) 134320, <https://doi.org/10.1016/j.conbuildmat.2023.134320>.
- [10] A. Tokareva, S. Kaassamani, D. Waldmann, Fine demolition wastes as supplementary cementitious materials for CO2 reduced cement production, *Constr.*

- Build. Mater. 392 (2023) 131991, <https://doi.org/10.1016/J.CONBUILDMAT.2023.131991>.
- [11] T.C.F. Oliveira, B.G.S. Dezen, E. Possan, Use of concrete fine fraction waste as a replacement of portland cement, *J. Clean. Prod.* 273 (2020) 123126, <https://doi.org/10.1016/J.JCLEPRO.2020.123126>.
 - [12] Z. Prošek, V. Nežerka, R. Hlůžek, J. Trejbal, P. Tesárek, G. Karra'a, Role of lime, Fly ash, and slag in cement pastes containing recycled concrete fines, *Constr. Build. Mater.* 201 (2019) 702–714, <https://doi.org/10.1016/J.CONBUILDMAT.2018.12.227>.
 - [13] J. Moreno-Juez, I.J. Vegas, M. Frías Rojas, R. Vigil de la Villa, E. Guede-Vázquez, Laboratory-scale study and semi-industrial validation of viability of inorganic CDW fine fractions as SCMs in blended cements, *Constr. Build. Mater.* 271 (2021) 121823, <https://doi.org/10.1016/J.CONBUILDMAT.2020.121823>.
 - [14] Standard Practice for Classification of Soils for Engineering Purposes (Unified Soil Classification System) 1, n.d. www.astm.org
 - [15] W.Ten Kuo, Z.C. Gao, Engineering properties of controlled low-strength materials containing bottom ash of municipal solid waste incinerator and water filter silt, *Appl. Sci.* 8 (2018), <https://doi.org/10.3390/app8081377>.
 - [16] C. Lampris, R. Lupo, C.R. Cheeseman, Geopolymerisation of silt generated from construction and demolition waste washing plants, *Waste Manag.* 29 (2009) 368–373, <https://doi.org/10.1016/j.wasman.2008.04.007>.
 - [17] F.C. Chang, M.Y. Lee, S.L. Lo, J.D. Lin, Artificial aggregate made from waste stone sludge and waste silt, *J. Environ. Manag.* 91 (2010) 2289–2294, <https://doi.org/10.1016/j.jenvman.2010.06.011>.
 - [18] I.A. Verkhovets, N.P. Chizhikova, A.S. Vladychenskii, Mineralogical composition of silt fractions and its transformation under the impact of different cenoses in model lysimeters, *Eurasia Soil Sci.* 39 (2006) 528–538, <https://doi.org/10.1134/S1064229306050103>.
 - [19] S. Pu, Z. Zhu, L. Zhao, W. Song, Y. Wan, W. Huo, H. Wang, K. Yao, L. Hu, Microstructural properties and compressive strength of lime or/and cement solidified silt: a multi-scale study, *Bull. Eng. Geol. Environ.* 79 (2020) 5141–5159, <https://doi.org/10.1007/s10064-020-01910-y>.
 - [20] S. Maruthupandian, A. Chaliasou, A. Kanellopoulos, Recycling mine tailings as precursors for cementitious binders – methods, challenges and future outlook, *Constr. Build. Mater.* 312 (2021) 125333, <https://doi.org/10.1016/j.conbuildmat.2021.125333>.
 - [21] Sid 5, New technologies to allow beneficial reuse of silt from construction and demolition waste recycling washing plant, Research Project Report (WR0204 (WRT 236)) Submitted to Defra, Science Directorate 5 (2009) 1–25.
 - [22] C. Lampris, R. Lupo, C.R. Cheeseman, Geopolymerisation of silt generated from construction and demolition waste washing plants, *Waste Manag.* 29 (2009) 368–373, <https://doi.org/10.1016/j.wasman.2008.04.007>.
 - [23] Agg-net, New recycling centre for Eco Aggregates | Agg-Net, (n.d.). <https://www.agg-net.com/news/new-recycling-centre-for-eco-aggregates> (accessed March 28, 2023).
 - [24] The Munsell Color System, (n.d.). <http://www.applepainter.com/> (accessed July 4, 2022).
 - [25] T. Degen, M. Sadki, E. Bron, U. König, G. Nénert, The HighScore suite, *Powder Diff.* 29 (S2) (2014) S13–S18, <https://doi.org/10.1017/S0885715614000840>.
 - [26] G. Yao, Q. Liu, J. Wang, P. Wu, X. Lyu, Effect of mechanical grinding on pozzolanic activity and hydration properties of siliceous gold ore tailings, *J. Clean. Prod.* 217 (2019) 12–21, <https://doi.org/10.1016/j.jclepro.2019.01.175>.
 - [27] H. Shin, S. Lee, H. Suk Jung, J.B. Kim, Effect of ball size and powder loading on the milling efficiency of a laboratory-scale wet ball mill, *Ceram. Int.* 39 (2013) 8963–8968, <https://doi.org/10.1016/j.ceramint.2013.04.093>.
 - [28] P. Perumal, K. Piekkari, H. Sreenivasan, P. Kinnunen, M. Ilkainen, One-part geopolymers from mining residues – effect of thermal treatment on three different tailings, *Min. Eng.* 144 (2019) 106026, <https://doi.org/10.1016/j.mineng.2019.106026>.
 - [29] S. Ramanathan, REACTIVITY OF SUPPLEMENTARY CEMENTITIOUS MATERIALS IN MODEL SYSTEMS AND CEMENTITIOUS PASTES, PhD Thesis Submitted to University of Miami (2021) 249.
 - [30] F.C. Chang, M.Y. Lee, S.L. Lo, J.D. Lin, Artificial aggregate made from waste stone sludge and waste silt, *J. Environ. Manag.* 91 (2010) 2289–2294, <https://doi.org/10.1016/j.jenvman.2010.06.011>.
 - [31] Lea's Chemistry of Cement and Concrete, Elsevier, 2019. <https://doi.org/10.1016/C2013-0-19325-7>.
 - [32] K. Scrivener, R. Snellings, B. Lothenbach, *A Practical Guide to Microstructural Analysis of Cementitious Materials*, 1st ed., CRC Press, Taylor and Francis Group, 2016.
 - [33] M.M.H. Al Omari, I.S. Rashid, N.A. Qinna, A.M. Jaber, A.A. Badwan, Calcium Carbonate, 2016. <https://doi.org/10.1016/bs.podrm.2015.11.003>.
 - [34] Ö. Bozkaya, H. Yalçın, M.C. Gönçüoğlu, Diagenetic and very low-grade metamorphic characteristics of the paleozoic series of the Istanbul terrane (NW Turkey), *Swiss J. Geosci.* 105 (2012) 183–201, <https://doi.org/10.1007/s00015-012-0108-2>.
 - [35] R. Zhao, Z.C. Tian, Z. Zhao, Effect of calcination temperature on rare earth tailing catalysts for catalytic methane combustion, *Green. Process. Synth.* 9 (2020) 734–743, <https://doi.org/10.1515/gps-2020-0053>.
 - [36] K. Peng, H. Yang, J. Ouyang, Tungsten tailing powders activated for use as cementitious material, *Powder Technol.* 286 (2015) 678–683, <https://doi.org/10.1016/j.powtec.2015.09.012>.
 - [37] K. Berent, S. Komarek, R. Lach, W. Pyda, The Effect of Calcination Temperature on the Structure and Performance of Nanocrystalline Mayenite Powders, (2019).
 - [38] R. Fernandez, F. Martirena, K.L. Scrivener, The origin of the pozzolanic activity of calcined clay minerals: a comparison between kaolinite, illite and montmorillonite, *Cem. Concr. Res.* 41 (2011) 113–122, <https://doi.org/10.1016/j.cemconres.2010.09.013>.
 - [39] D. Zhou, Developing supplementary cementitious materials from waste London clay, Imperial College London, 2016, p. 236. (<https://spiral.imperial.ac.uk/handle/10044/1/44528>).
 - [40] M. Ilkainen, P. Perumal, J. Kiventer, Influence of alkali source on properties of alkali activated silicate tailings 271 (2021), <https://doi.org/10.1016/j.matchemphys.2021.124932>.
 - [41] Gypsum – Database of ATR-FT-IR spectra of various materials, (n.d.). (<https://spectra.chem.ut.ee/paint/fillers/gypsum/>) (accessed April 18, 2024).
 - [42] N. Sedira, J. Castro-Gomes, Effect of activators on hybrid alkaline binder based on tungsten mining waste and ground granulated blast furnace slag, *Constr. Build. Mater.* 232 (2020) 117176, <https://doi.org/10.1016/j.conbuildmat.2019.117176>.
 - [43] K. Komnitsas, D. Zaharaki, Geopolymerisation: a review and prospects for the minerals industry, *Min. Eng.* 20 (2007) 1261–1277, <https://doi.org/10.1016/j.mineng.2007.07.011>.
 - [44] Y.M. Liew, H. Kamarudin, A.M. Mustafa Al Bakri, M. Bnhussain, M. Luqman, I. Khairul Nizar, C.M. Ruzaidi, C.Y. Heah, Optimization of solids-to-liquid and alkali activator ratios of calcined kaolin geopolymeric powder, *Constr. Build. Mater.* 37 (2012) 440–451, <https://doi.org/10.1016/j.conbuildmat.2012.07.075>.
 - [45] I. Silva, J.P. Castro-Gomes, A. Albuquerque, Effect of immersion in water partially alkali-activated materials obtained of tungsten mine waste mud, *Constr. Build. Mater.* 35 (2012) 117–124, <https://doi.org/10.1016/j.conbuildmat.2012.02.069>.
 - [46] I.O. Faniyi, O. Fasakin, B. Olofinjana, A.S. Adekunle, T.V. Oluwasusi, M.A. Eleruja, E.O.B. Ajayi, The comparative analyses of reduced graphene oxide (RGO) prepared via Green, mild and chemical approaches, *SN Appl. Sci.* 1 (2019) 1–7, <https://doi.org/10.1007/s42452-019-1188-7>.
 - [47] S. Hollanders, Mineralogical study of the pozzolanic properties of calcined clays, (2017) 236. https://limo.libis.be/primo-explore/fulldisplay?docid=LIRIAS1727587&context=L&vid=Lirias&search_scope=Lirias&tab=default_tab&lang=en_US&fromSitemap=1.
 - [48] S.J. Kemp, A.L. Lewis, J.C. Rushton, Detection and quantification of low levels of carbonate mineral species using thermogravimetric-mass spectrometry to validate CO₂ drawdown via enhanced rock weathering, *Appl. Geochem.* 146 (2022) 105465, <https://doi.org/10.1016/J.APGEOCHEM.2022.105465>.
 - [49] N. Yoobanpot, P. Jamsawang, H. Poorahong, P. Jongpradist, S. Likitlersuang, Multiscale laboratory investigation of the mechanical and microstructural properties of dredged sediments stabilized with cement and Fly ash, *Eng. Geol.* 267 (2020) 105491, <https://doi.org/10.1016/J.ENGGEOL.2020.105491>.
 - [50] S. Ramanathan, L.R. Pestana, P. Suraneni, Reaction kinetics of supplementary cementitious materials in reactivity tests, *Cement* 8 (2022) 100022, <https://doi.org/10.1016/j.cement.2022.100022>.